Mitigating Rayleigh Taylor Instabilities in the Deceleration Phase of Inertial Confinement Fusion

John Giess

McQuaid Jesuit High School

LLE Advisors: Dr. Valeri Goncharov, Dr. Ka Ming (Jack) Woo

April 2023

Laboratory for Laser Energetics
University of Rochester

1 Abstract

The Rayleigh Taylor (RT) hydrodynamic instability can reduce the temperature in the hot spot and limit target performance in inertial confinement fusion. The RT instability is formed when a lower density material pushes on a higher density material. RT growth amplifies shell imperfections at the outer surface during the shell acceleration and at the inner surface during the deceleration. We investigated mitigation techniques for RT perturbation amplification in the deceleration phase. These include the mistiming of shocks to increase the entropy and reduce the density at the inner part of the shell. These shocks propagate into the shell at the beginning of the implosion. In a nominal design, the shocks are timed so they all merge at the shell's inner surface. We changed the height of the foot during the early part of the laser pulse in order to see the effect of the shocks merging inside the shell. We then calculated the RT growth rate using the change in the density scale length and the inner radius. We found a design with a high foot that has a larger density scale length and limits RT growth.

2 Introduction

2.1 Inertial Confinement Fusion

At the 60-beam OMEGA Laser Facility, inertial confinement fusion (ICF) implosions are created with direct beam irradiation on a spherical cryogenic target. In this process, extremely high densities, pressures and temperatures are reached allowing for the fusion of particles in the inner core of the target. The target typically contains a combination of deuterium and tritium (DT), two hydrogen isotopes, in a gaseous form at the center of the target and in a frozen form surrounding this gas. A layer of plastic, glass or other material encloses the target forming an outermost layer. For the purposes of this study, a plastic layer, which is known as an ablator, was used and two different targets with different layers were used for simulation. However, these targets will not be perfectly spherical as they often have imperfections that are amplified through the ICF implosion. In the beginning of an ICF implosion, the laser irradiation is absorbed in the outer shell layer resulting in the ablation of the outer material. This force accelerates the target's shell inward. The shell then moves into the deceleration phase as the low density plasma hotspot region in the center pushes against the higher density outer region. The target's shell is slowed down during the deceleration phase as return shocks move through the shell. The shell continues to compress and the internal gas grows in temperature creating a "hot spot" region where fusion reactions can occur. After the shell decelerates, peak compression occurs. Bang time, the time at which the fusion rate is maximum, occurs when the fuel reaches maximum compression and this is often called the stagnation point. In this phase, if the self heating rate through alpha particle deposition is greater than the energy loss rate within the hot spot, a burning plasma state occurs that triggers an unstable thermonuclear burn wave. Much higher temperatures and neutron yields are the result. A burn state is required to reach ignition where output exceeds input energy.

2.2 Rayleigh-Taylor Growth

We can see the effects of Rayleigh Taylor (RT) instability, which occurs when a lower density material pushes on a higher density material. It leads to exponential growth in perturbations. It first occurs on the outer surface of the target during the acceleration phase. Perturbations are amplified as the lower density laser plasma pushes against the more dense outer shell. The instability also occurs later, during the deceleration phase. The RT growth is undesirable for two reasons. First, during the compression, the shell's kinetic energy is wasted to amplify perturbations instead of uniformly compressing the target. Second, by the time of peak compression, the cold dense shell mixes with the inner hot spot region lowering its temperature and therefore lowering the fusion reaction rates.

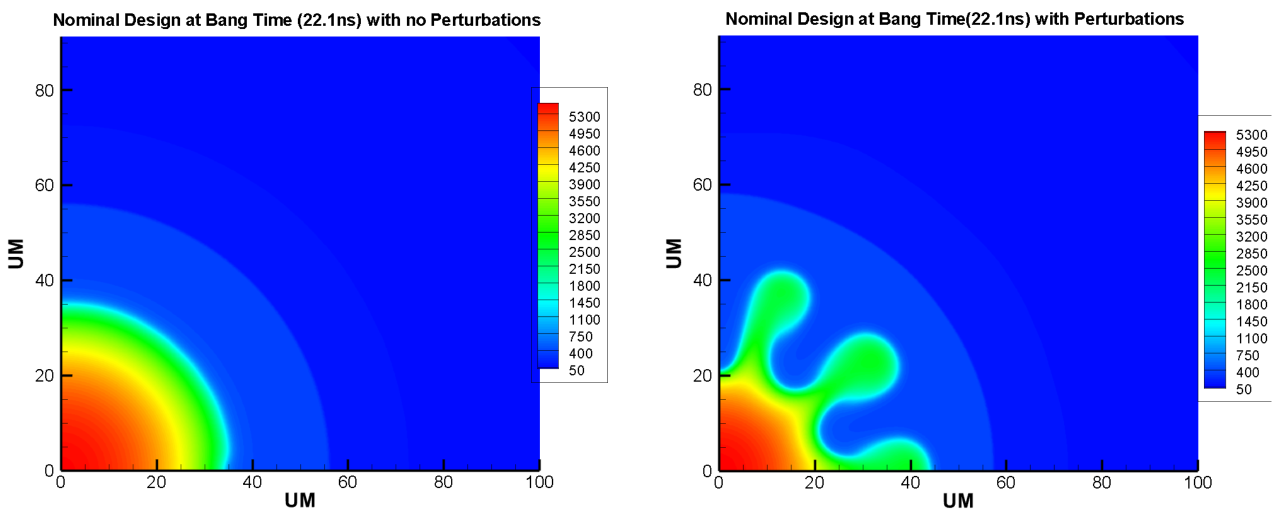

(a) (b)

Figure 1. (a) Temperature contours (in eV) at bang time for a target simulated using the code DEC2D with no RT perturbations. (b) Temperature contours at bang time for a target with RT perturbations. This target has a lower internal temperature. (The temperature scale is the same for both figures)

The RT instability is illustrated in Figure 1 for two simulations, one (Figure 1a) for a target without perturbations and the other (Figure 1b) for a target with perturbations. These temperature contour plots are shown at bang time with distances in μm using Cartesian geometry. The simulations were done by first running the 1D radiation-hydrodynamics code LILAC [1] for the entire length of the pulse. Profiles of required data were transferred to the 2D simulation code DEC2D [2] at the beginning of the deceleration phase and a perturbation on the density, pressure, or temperature with a selected mode number was then added. DEC2D followed the implosion through the deceleration phase to slightly after the bang time. The green fingers are where there is higher temperature and between them the blue fingers indicate higher density. The target imploded contained an inner gaseous DT region of radius 850 μm, enclosed by a frozen DT region which is 450 μm thick, followed by a thin outer plastic shell which is 110 μm thick. The pulse shape used is shown in Figure 2. We can see the decrease in size of the hot spot at bang time, the area inside the yellow contour in Figure 1, whose radius is approximately 1.8% of the size of the initial target's radius 1410 μm, as it is around 25 μm in Figure 1(a) and 17.5 μm in Figure 1(b).

2.3 Adiabat Shaping

There are many techniques to reduce RT growth. The approach we analyzed was changing the shape of the pulse. [3] One method is called a decaying shock, where a prepulse causes a decaying shock in the shell. Another is the relaxation method, where a prepulse is used and the adiabat is shaped by the foot of the main pulse.[4] This adiabat, defined as the pressure divided by the Fermi pressure (the minimum pressure due to degeneracy), is given by the equation [5],

$$\alpha = \frac{P(Mb)}{2.18\rho(g/cc)^{5/3}}$$

with the pressure (P) given in megabars and the density (ρ) given in (g/cc). A higher adiabat means that we will have higher internal temperatures which would lower the density gradient and limit RT growth. We can change the adiabat to cause these conditions by using various shaping techniques which modify the pressure and density in different regions.

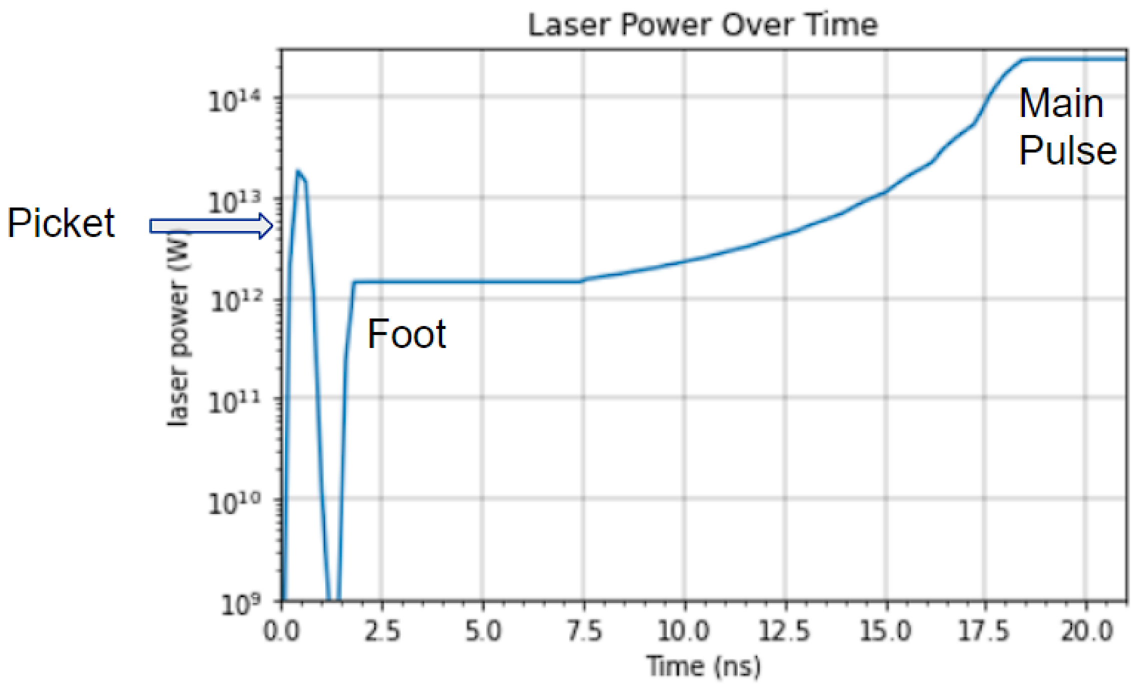

Figure 2. The initial laser pulse design used, with the strong prepulse (picket), foot (that drives a supported shock) and main pulse labeled. The main pulse continues until 22.5 ns. The foot is characterized by a power of 1.45 TW.

Our design used the laser pulse shown in Figure 2, which included a picket, a foot, and a main pulse that is ramped up to and begins at 18.6 ns. Both the height and duration of the foot and picket can be changed by adjusting the laser power. Through studies of 1D LILAC simulations, we decided to focus on modifying the height of the foot, leaving the picket pulse unchanged, to shape the adiabat. In the nominal design, the height and start time of the foot and the picket were arranged so that these two shocks would merge at the shell's inner surface. We looked at the effect of raising the height, or laser power, of the foot, so that the shocks would instead merge inside of the shell of the target.

2.4 Rayleigh-Taylor Growth Calculations

The main goal of these shaping techniques is to reduce the RT growth, which can be linearly modeled by the equation,

$$perturbation\ growth = exp \int_{t_{Begin}}^{t_{End}} \gamma\, dt$$

where the growth rate is given by

$$\gamma = \sqrt{\frac{kg}{1 + kL}}$$

with $k = \frac{2\Pi}{\lambda}$ where λ is the wavelength of the perturbation, $\lambda = \frac{2\Pi R}{l}$ where l is the mode number (the number of wavelengths going around the circumference), R is the shell radius and *L* is the minimum value of the density gradient scale length at the unstable interface, which for the deceleration instability is the boundary between the hot spot and the imploding shell. The quantity g is the shell acceleration or deceleration and is analogous to gravity. The beginning time t_{Begin} is the start of the deceleration phase and the end time t_{End} is bang time. By using this formula, if we are able to maximize the density scale length, we can therefore minimize the growth of perturbations if the duration of the acceleration phase does not change. This can be done by reducing the difference in densities between the hot spot and the imploding shell through adiabat shaping techniques. However, if the time it takes to reach the bang time increases with the increase in density scale length, the perturbations will have more time to grow, therefore minimizing the effect of a larger density gradient scale length.

2.5 Simulations

Two different simulation codes were used to evaluate the effects of our adiabat shaping techniques. The first used was LILAC. By simulating different input laser pulse shapes and target conditions this code allowed us to view the effect of the shocks through changes in pressure and density over time. By modifying both of these inputs, the energy output (neutron yield) and changes in bang time (the stagnation point) could be quickly analyzed to compare with early designs. Profiles of promising 1D simulations were then imported into DEC2D using output from the LILAC simulation at the beginning of the deceleration phase and the addition of a 2D perturbation. DEC2D allows us to directly analyze the effects of these perturbations. The sizes of the perturbations were then measured over time, which allowed for a comparison of the results from the different designs.

3 Initial Optimizations

3.1 Initial Parameters and Shell Design

For these tests a NIF-scale implosion was simulated. The initial target design contains an inner gaseous DT region of radius 850 μm, enclosed by a frozen DT region which is 450 μm thick, followed by a thin outer plastic shell which is 110 μm thick. Burn conditions would begin when the neutron yield was around 10^{17} and this would lead to a rapid increase in the yield to around 10^{19}. As shown in Figure 2, the length of the laser pulse was 22.5 ns with a picket, a foot pulse, and a main pulse with a maximum power of 240 TW. In order to achieve a greater density scale length the height of the foot pulse was systematically increased in LILAC simulations.

3.2 1D simulation results

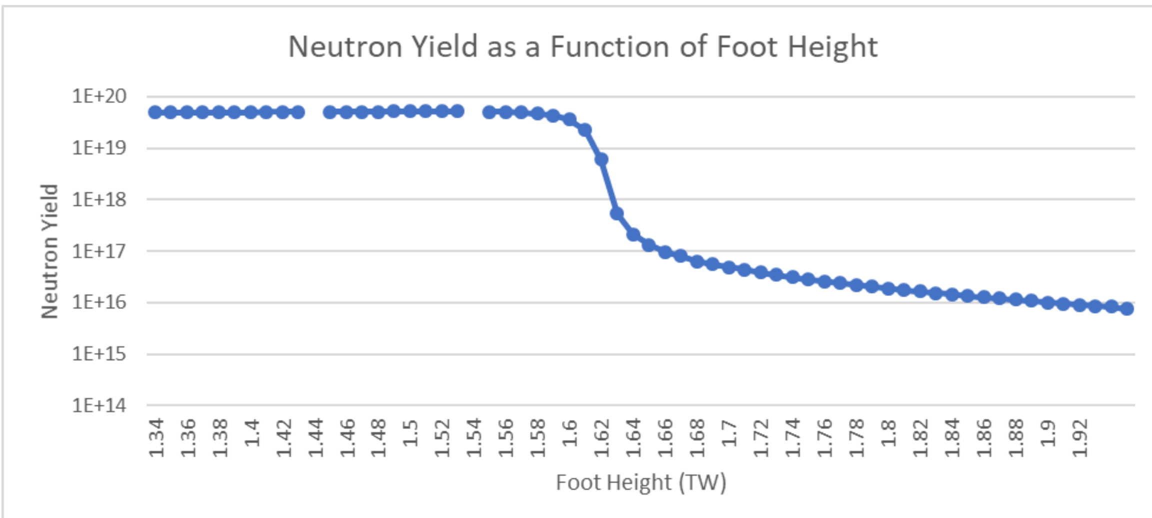

Figure 3. The neutron yield as a function of the power in the foot. Each dot represents an increase in the height of the foot by 10 GW.

As seen in Figure 3 the neutron yield decreased slightly as the height of the foot increased until the height of the foot reached 1.62 TW, where the neutron yield had a steep drop off. This drop off represents the target not reaching burn conditions. Through this initial round of testing we identified the range of possible foot heights to be from 1.45 to 1.62 TW. Also, as the height of the foot increased, so did the density scale length. We ruled out foot heights lower than 1.45 TW, which was the foot height in our nominal design, because when the heights were lowered from the nominal height the density scale length decreased. Our best design increased the average density scale length from 2.3 to 3.6 μm. This is promising because 1D LILAC simulations are not affected by the perturbations. So even though the 1D simulations showed a lower neutron yield or output, it is likely that the increased scale length could lead to reduced perturbations and therefore more stability in the 2D simulations.

3.3 2D simulation results

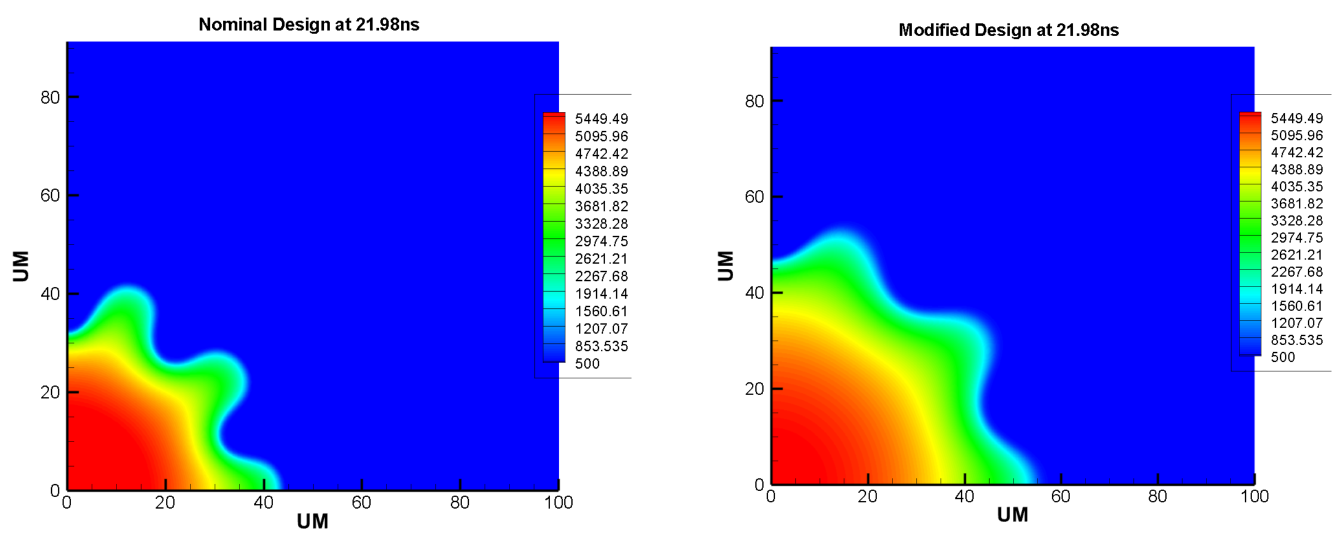

Figure 4. Temperature contours at 21.98 ns for the nominal design, the initial design (left) and the modified design, the higher foot design (right). The temperature is plotted in electron volts.

The anticipated improvements were indeed seen in the 2D simulations, where the rate of growth of the perturbations was greatly decreased in the higher foot designs by the increased density scale lengths at similar times. This can be seen in Figure 4, which compares the temperature contours for the nominal design (foot height 1.45 TW) and a modified design (foot height 1.61 TW) at the same time (21.98 ns). The perturbations are much smaller in the modified design. However, the problem was that the bang time increased by 0.22 ns. This time increase was because the target became harder to compress. As a result, the perturbations had significantly more time to grow in all of the higher foot designs and eventually became larger than the perturbations in the nominal design.

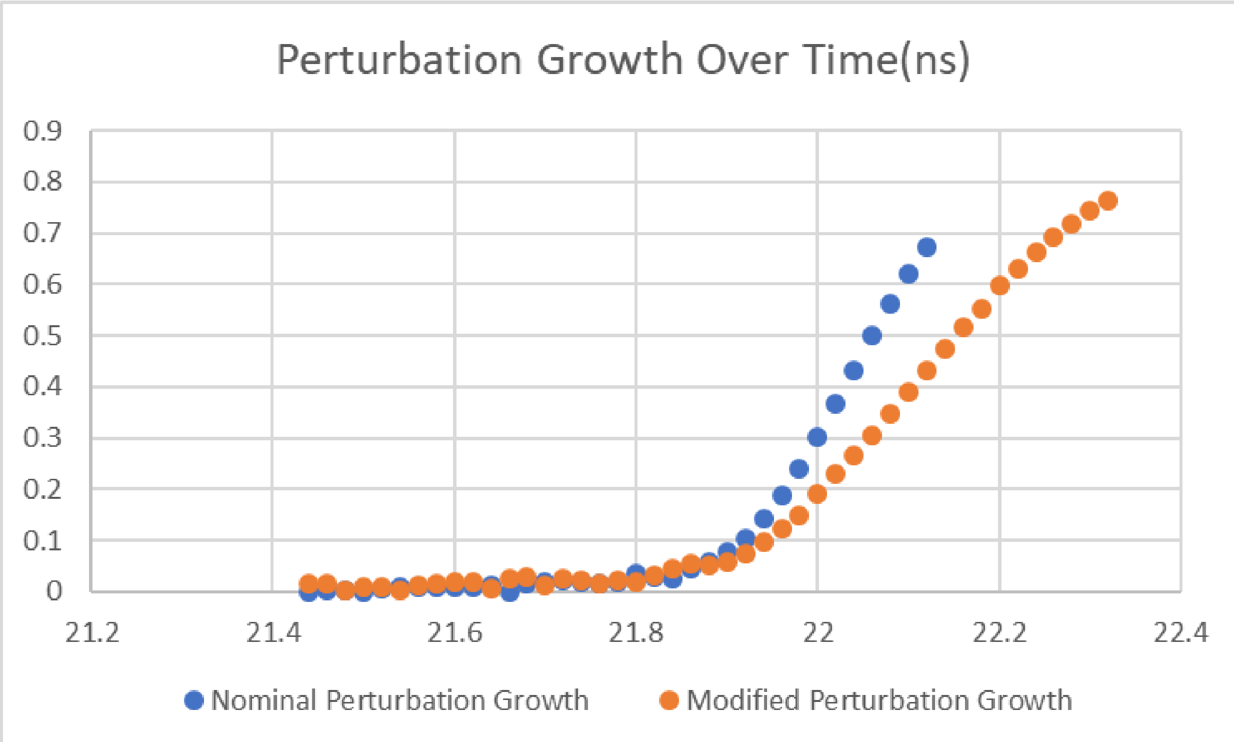

Figure 5. Perturbation growth for the nominal and modified (higher foot) designs as a function of time(ns). The data begin at the start of the decceleration phase at 21.44ns and end at bang time. Perturbation growth is calculated as the radius to the edge of the perturbation divided by the perturbation wavelength.

This is illustrated in Figure 5, which plots the perturbation growth as a function of time for the nominal and modified designs ending at bang time. The edge of the perturbation can be seen in Figure 4 where the temperature contour shows light blue. It is seen that the nominal design had less growth than the higher foot design by the time they both reached bang time. It can therefore be concluded that the increase in foot height can lead to a decrease in the rate of perturbation growth because of the lower density slope, but an increase in the bang time. Using these results we hypothesized that if we could decrease the time it takes for the target to implode using a modified target design we could mitigate this increase in time and utilize the improved scale length and growth rate to have less total perturbation growth.

4 Improved Shell Design

4.1 Parameters and 1D Results

The new shell design had a much smaller DT ice region of 180 μm thickness (reduced from 450 μm) with a gaseous region of radius 1305 μm (increased from 850 μm), so that it would implode earlier than the previous design. The plastic layer was kept at the same thickness of 110 μm to absorb the laser and ablate off, causing the inward shell acceleration.

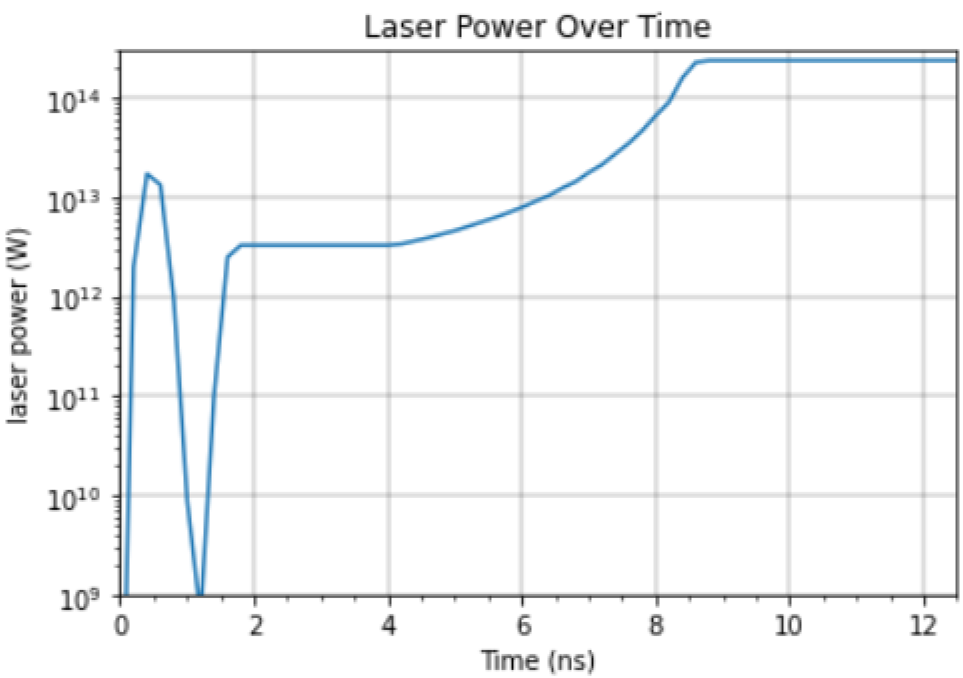

Figure 6. The shorter laser pulse for the thinner shell design.

The nominal laser pulse design was modified along with the shell to be much shorter to account for the quicker implosion (see Figure 6). The heights of the main laser pulse and picket were the same as in the previous design (Figure 2). Using this new design, multiple foot height changes were simulated with LILAC. These initial simulations showed a large increase in density scale length compared with the nominal design as well as only slight bang time increases. The average density scale length from the start of deceleration to bang time was almost double in the thinner-shell design.

4.2 Results

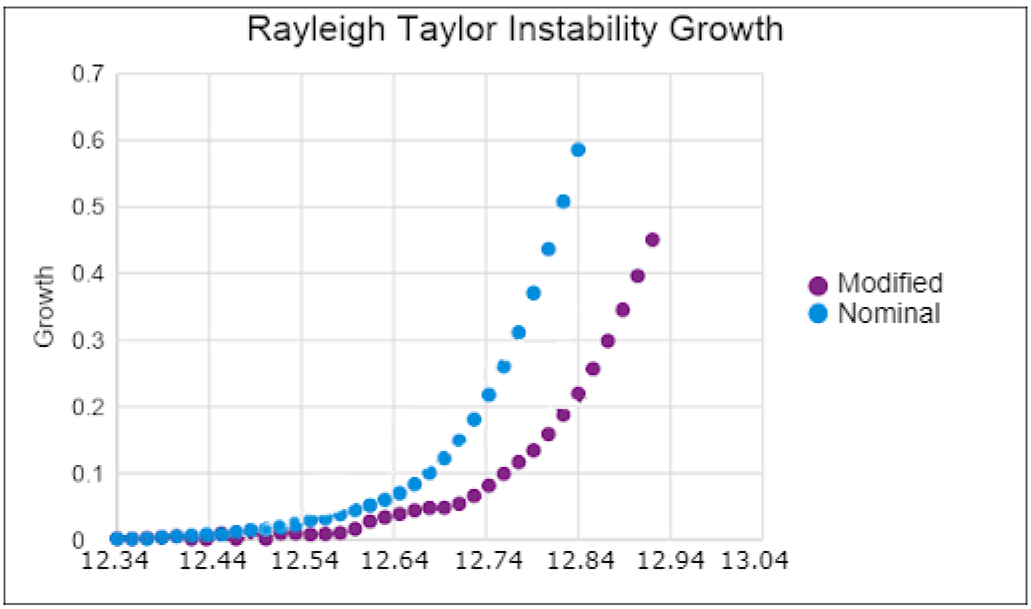

Figure 7. Perturbation growth for the nominal and modified (higher foot) designs as a function of time (ns) for the shorter laser pulse. As in Figure 5, the data runs from the start of deceleration until the bang time. Here the modified design has a later bang time, but smaller overall growth.

Similarly to Section 3 we considered two pulse shapes: nominal (foot height 3.7 TW) and modified (foot height 5 TW). Figure 7 is the same as Figure 5, but for the shorter laser pulse. It shows that although our higher foot design took longer to reach bang time the perturbation growth was still ultimately less than for the nominal design. Therefore, because the perturbation growth was minimized while still reaching burn conditions, the design became more stable due to the much higher density scale length.

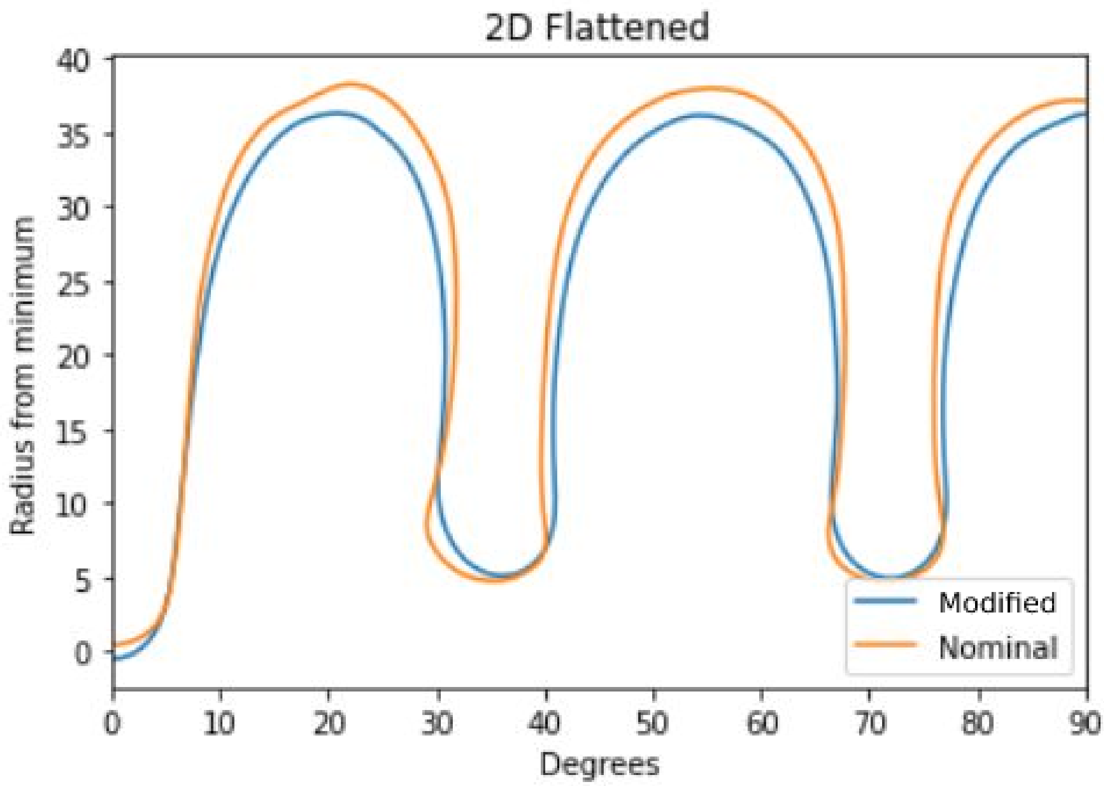

Figure 8. A flattened comparison of the perturbations in the nominal design (orange) and the modified design (blue) of Figure 7 at bang time, plotted against angle from the vertical in the temperature contour plot. Perturbation radius from the minimum is calculated as the distance from the center to the edge of the perturbation minus the lowest part of the perturbation for a DEC2D plotted temperature contour. This is illustrated in Figure 1(b) where the maximum radius of the perturbation would be approximately 42 µ*m and the lowest part of the perturbation is 21* µ*m.*

Figure 8 shows that there was a reduction in the RT growth; however, due to the time increase this reduction is very minimal. Also, this higher foot design had a slightly lower neutron yield output. The curves show a minimal reduction while Figure 7 shows a greater reduction because the results in Figure 7 used a higher initial perturbation level than the simulation shown in Figure 8. This shows that at higher levels of perturbation the reduction techniques have a greater mitigating effect in relation to the nominal design.

To further improve the design, more precise tunings could first be used. This could be done through utilization of a neural network or gradient descent optimization while modifying the height and space between the picket and the foot. Other modifications, such as the type of outer plastic as well as different target shapes, could be used to help with stability and neutron output.

6 Conclusions

RT growth leads to a waste of the shell's kinetic energy that could otherwise be used to compress the hotspot and a cooling effect within the hot spot region. To reduce the growth of these perturbations, adiabat tuning methods can be used. We modified the height of the foot to make the shocks merge in the shell of the target, increasing the density scale length and reducing the RT growth rate. Different foot heights were simulated in 1D simulations that still reached burn conditions. The density scale length was found to increase as expected. However, 2D simulations showed that while the density scale length was increased and the growth rate was decreased, the implosion took longer, which meant that the total growth of the perturbations increased. Through the use of a new, thinner DT ice layer, a higher foot design was developed that decreased the RT growth rate and also had an earlier bang time than the previous designs. This design showed a slight perturbation reduction, but due to the substantial increase in density scale length for these higher foot designs, additional optimization could be used to produce a larger perturbation reduction.

7 Acknowledgements

Massive thanks to Dr. Woo and Dr. Goncharov. They spent countless hours teaching me about the fundamentals of fusion and shockwaves and mentored me throughout this project. Dr. Woo also spent additional time helping me learn Python and the various simulators. Many thanks to Dr. Craxton for the time he put in to organize the program. I would also like to thank Ms. Truebger for helping to make the program run smoothly as well as Yousef Lawrence for his initial guidance and materials. Lastly, thanks to all of the other students in the program for their help and making the eight weeks of the summer so enjoyable.

8 References

1. J. Delettrez, R. Epstein, M. C. Richardson, P. A. Jaanimagi, and B. L. Henke, "Effect of Laser Illumination Nonuniformity on the Analysis of Time-Resolved X-Ray Measurements in UV Spherical Transport Experiments," Phys. Rev. A **36** (8), 3926-3934 (1987).
2. K. M. Woo, R. Betti, D. Shvarts, A. Bose, D. Patel, R. Yan, P.-Y. Chang, O. M. Mannion, R. Epstein, J. A. Delettrez, M. Charissis, K. S. Anderson, P. B. Radha, A. Shvydky, I. V. Igumenshchev, V. Gopalaswamy, A. R. Christopherson, J. Sanz, H. Aluie. (2018) Effects of residual kinetic energy on yield degradation and ion temperature asymmetries in inertial confinement fusion implosions. *Physics of Plasmas* 25:5, 052704.

3. K.S. Anderson. *Adiabat shaping in direct-drive inertial confinement fusion implosions*. Ph. D. thesis, University of Rochester, New York, Jan. 2006.
4. R. Betti, K. Anderson, J. Knauer, T. J. B. Collins, R. L. McCrory, P. W. McKenty, S. Skupsky. (2005) Theory of laser-induced adiabat shaping in inertial fusion implosions: The relaxation method. *Physics of Plasmas* **12**:4, 042703.
5. S. Atzeni and J. Meyer-ter-vehn, The Physics of Inertial Fusion: Beam Plasma Interaction, Hydrodynamics, Hot Dense Matter, International Series of Monographs on Physics (Oxford University Press, Oxford, 2004).